Electric-field-gradient calculations on cadmium in cadmium-helium vacancy clusters in tungsten

D. P. van der Werf*
Nuclear Solid State Physics, Material Science Centre, University of Groningen, Nijenborgh 4, 9747 AG Groningen, The Netherlands

H. van Leuken and R. A. de Groot
Electronic Structure of Materials, Research Institute for Materials, Catholic University of Nijmegen, Toernooiveld 1, 6525 ED Nijmegen, The Netherlands

(Received 17 February 1995)

Electric-field gradients (EFG) at the position of the cadmium atom in low-symmetry CdV_nHe_m clusters in tungsten were calculated with the augmented spherical wave method. The results agreed within 70% with experimental values. It is observed that lattice relaxation has a large effect on both the quadrupole frequency ω_0 and the asymmetry parameter η. The value of η for the unrelaxed clusters CdV_2 and CdV_3He_2 are not equal to 1.0, as predicted by the point charge model. The cluster CdV_2He_2 has a temperature-dependent EFG with a transition temperature of about 100 K. The same holds for CdV_3He_4, but in this case there are two transitions, at abut 170 and 250 K, respectively.

I. INTRODUCTION

Perturbed angular correlation (PAC) measurements of the electric-field gradient (EFG) at probe atoms in materials can be of great help to identify the immediate surrounding of these atoms. The results of such measurements are often compared with those obtained with techniques such as thermal helium desorption spectroscopy, channelling, extended x-ray-absorption fine structure, low-energy ion scattering, and a number of other techniques which are sensitive to the configuration of small defects. Theoretical predictions of the EFG are needed in order to give a reliable and unambiguous interpretation of the experimental data. Several more or less successful attempts have been made to calculate the EFG using either the point charge model,[1] *ab initio* band-structure calculations,[2,3,4] or cluster calculations.[5] These EFG calculations were most times (except for cluster calculations[6]) only performed for compounds or highly symmetrical surrounding of the probe atom.[7]

In this paper the results of EFG calculations that were performed using the augmented spherical wave (ASW) method[8] are presented. The calculations are restricted to a number of low-symmetry cadmium-vacancy and cadmium-vacancy-helium clusters in tungsten which we recently have investigated by means of PAC.[9] One should keep in mind that vacancies and helium atoms were trapped at the radioactive atom ^{111}In which decays to ^{111}Cd. The lattice around ^{111}Cd will relax within a time of the order of 100 fs, while a typical PAC spectrum spans a time interval of the order of 100 ns. Therefore, we have used the atom positions calculated with the atom embedding method of Finnis and Sinclair.[10]

The paper is organized as follows. In Sec. II we give a few expressions that describe the EFG and its relation with the measured PAC frequencies. More information about this subject can be found in the review article written by Kaufman and Vianden.[11] The conversion from frequency to EFG suffers from the uncertainty in the nuclear quadrupole moment of the $5/2^+$ state of ^{111}Cd, as explained in Sec. III. In Sec. IV we briefly outline the procedure of how to calculate the EFG using the ASW method. In Sec. V we present the results of molecular statics and molecular dynamics simulations that were performed to study the atom positions and their fluctuations. Calculated EFG values are presented in Sec. VI. The discussion is held in Sec. VII, and we conclude this chapter with some remarks in Sec. VIII.

II. THE ELECTRIC-FIELD GRADIENT

The electric-field gradient is defined as the second partial derivative of the electrostatic potential Φ:

$$V_{ab}=\frac{\partial^2\Phi}{\partial a\,\partial b} \tag{1}$$

for $a,b=x,y,z$. It is a symmetric second rank tensor, the trace of which is zero because of Laplace's equation, $\nabla^2\Phi=0$, and it can be diagonalized by a rotation of the coordinate system towards the principal axes system (PAS). Conventionally, the PAS is chosen in such a way that $|V_{xx}|\le|V_{yy}|\le|V_{zz}|$. The EFG tensor is then completely determined by its principal component V_{zz}, the asymmetry parameter

$$\eta=\frac{V_{xx}-V_{yy}}{V_{zz}}\ , \tag{2}$$

and the three Euler angles that describe the orientation of the PAS. We note that $V_{zz}=0$ in a cubic environment, and that a threefold symmetry axis gives rise to $\eta=0$, i.e., $V_{xx}=V_{yy}$. In this case $V_{zz}=-2V_{xx}$ because of Laplace's equation.

The quadrupole frequency ω_0, measured in a perturbed angular correlation experiment, is related to the values of V_{zz} and η at the position of the probe atom:

$$\omega_0=\frac{2\pi n\nu_Q}{4I(2I-1)}f_I(\eta)\ . \tag{3}$$

The frequency ν_Q is defined as

$$\nu_Q = \frac{eQV_{zz}}{h} , \quad (4)$$

where Q is the nuclear quadrupole moment, I is the nuclear spin, and e is the unit of charge. In Eq. (3) $n=3$ if I is an integer, and $n=6$ if I is a half-integer. The function $f_I(\eta)$ depends on the value of I, but cannot be described by a simple analytical expression.[12] In our experiments we have used the probe ^{111}Cd, which has a nuclear spin of $I=5/2^+$ and a quadrupole moment of 0.83(13) b (see next section). In that case Eq. (3) becomes

$$\omega_0 = 1.9(3)\times 10^{-20} V_{zz} f_{5/2}(\eta) \text{ Mrad } s^{-1} , \quad (5)$$

with V_{zz} in V m^{-2}.

III. THE NUCLEAR QUADRUPOLE MOMENT OF THE $5/2^+$ STATE OF ^{111}Cd

The values reported for the nuclear quadrupole moment of ^{111}Cd($5/2^+$) vary from 0.44 to 1.5 b (see Table I). In the following we will discuss the reliability of the different values.

The first two quadrupole moments listed in Table I were derived by scaling the measured quadrupole frequencies according to the Sternheimer antishielding factors for Cd^{2+} and In^{3+}. It was implicitly assumed that the two probe atoms had the same electronic structure, and that the local lattice structure was not influenced by the impurity atom. Both assumptions are probably incorrect. Moreover, the point charge model, implicitly used, is inappropriate to describe the electric-field gradient in noncubic metals.[25,26] Therefore, we conclude that these values of the nuclear quadrupole moment are unreliable. The quadrupole frequency reported by Rosenblum and Steyert[17] is unreliable because their experiment suffered from faults in the thermometry.[22]

The next three quadrupole moments are based on the known nuclear quadrupole moments of the $5/2^+$ state in ^{109}Cd (Ref. 20) and the $11/2^-$ states in ^{111,113,115}Cd (Ref. 19). All these reference values have been derived using experimental and theoretical data from Lurio.[27] The errors in the three values of $Q(^{111}\text{Cd},5/2^+)$ are, therefore strongly correlated.

The last quadrupole moment quoted in Table I was derived using a theoretical value of the EFG for Cd in cad-

TABLE I. Reported values of $Q(^{111}\text{Cd},5/2^+)$.

Q (b)	Used data	Reference
0.44(7)	Measured ν_Q for ^{111}Cd($5/2^+$) in indium and for ^{115}In($9/2^+$) in indium, as functions of T	Bodenstedt *et al.* (Ref. 13)
	$\gamma_\infty(Cd^{2+})$ and $\gamma_\infty(In^{3+})$	Feiock and Johnson (Ref. 14)
	$Q(^{115}\text{In},9/2^+)=0.834$ b	quoted by Feiock and Johnson (Ref. 14)
0.77(12)	Measured ν_Q for ^{117}In($3/2^+$) and ^{111}Cd($5/2^+$) in several compounds and metals	Raghaven *et al.* (Ref. 15)
	$\gamma_\infty(Cd^{2+})$ and $\gamma_\infty(In^{3+})$	Feiock and Johnson (Ref. 14)
	$Q(^{117}\text{In},3/2^+)=0.64(4)$ b	Raghavan and Raghavan (Ref. 16)
1.5(4)	Measured $\nu_Q=-50(14)$ MHz for ^{115}Cd($11/2^-$) in cadmium	Rosenblum and Steyert (Ref. 17)
	Measured $\nu_Q=138(2)$ MHz for ^{111}Cd($5/2^+$) in cadmium	Raghaven *et al.* (Ref. 18)
	$Q(^{115}\text{Cd},11/2^-)=0.54(5)$ b	Geelhoed and McDermott (Ref. 19)
0.74(10)	Measured $\nu_Q=109.3(18)$ MHz for ^{111}Cd($5/2^+$) in cadmium and $\nu_Q=136.6(10)$ MHz for ^{109}Cd($11/2^-$) in cadmium	Sprouse *et al.* (Ref. 20)
	$Q(^{109}\text{Cd},11/2^-)=-0.92$ b extrapolated from the values of $Q(^{111,113,115}\text{Cd},11/2^-)$	Laulainen and McDermott (Ref. 21)
0.83(13)	Measured $\nu_Q=-139(15)$ MHz of ^{111}Cd($11/2^-$) in zinc	Herzog *et al.* (Ref. 22)
	Measured $\nu_Q=136.5(1.4)$ MHz for ^{111}Cd($5/2^+$) in zinc	Raghaven *et al.* (Ref. 18)
	$Q(^{111}\text{Cd},11/2^-)=-0.85(9)$ b	Laulainen and McDermott (Ref. 21)
0.80(10)	Measured $\nu_Q=102(12)$ MHz of ^{115}Cd($11/2^-$) in cadmium and $\nu_Q=110(4)$ MHz for ^{109}Cd($5/2^+$) in cadmium	Ernst *et al.* (Ref. 23)
	Measured $\nu_Q=136.02(41)$ MHz for ^{111}Cd($5/2^+$) in cadmium	Christiansen *et al.* (Ref. 24)
	$Q(^{115}\text{Cd},11/2^-)=0.54(5)$ b	Geelhoed and McDermott (Ref. 19)
	$Q(^{109}\text{Cd},5/2^+)=0.69(7)$ b	Laulainen and McDermott (Ref. 21)
0.74	$V_{zz}=7.62\times 10^{21}$ Vm^{-2} for Cd in cadmium	Blaha *et al.* (Ref. 25)
	Measured $\nu_Q=136.02(41)$ MHz for ^{111}Cd($5/2^+$) in cadmium	Christiansen *et al.* (Ref. 24)

mium. The EFG has been calculated with the aid of the fully linearized augmented plane waves (FLAPW) method,[25] which is considered as one of the most accurate *ab initio* methods available today. We conform ourselves to common practice and will use the value $Q(^{111}\mathrm{Cd},5/2^{+})=0.83(13)$ b, reported by Herzog *et al.*[22]

IV. CALCULATION: FROM ASW TO EFG

The ASW method[7] employs the atomic sphere approximation (ASA).[28] The crystal is divided in overlapping Wigner-Seitz spheres, centered at the atomic positions, with the only constraint that the total volume of the spheres equals the volume of the crystal. The potential inside a sphere is taken to be spherically symmetric. When the crystal contains two or more inequivalent atoms per unit cell, the Wigner-Seitz radii are not unique. In the ASA approximation, regions that below to several spheres contribute more than once to the total energy, while regions that belong to no sphere contribute nothing at all. The errors are expected to cancel to first approximation provided the potential varies slowly in the interstitial region, and the overlap between individual spheres is not too big. Although the potential is spherically symmetric, the wave functions derived from this potential are relatively well described.[3,4]

We distinguish three contributions to the EFG tensor. The first contribution, $V_{ab}(\mathrm{core})$, arises from polarized core electrons of the probe atom. The second contribution, $V_{ab}(\mathrm{val})$, originates from the valence electrons in the Wigner-Seitz sphere around the probe atom, and the third, $V_{ab}(\mathrm{lat})$, is due to the charge excess in the other Wigner-Seitz spheres.

We calculated $V_{ab}(\mathrm{val})$ in the following way. Consider a charge q at point $\mathbf{r}$. The electrostatic potential due to this charge is q/r. According to Eq. (1) the classical EFG tensor at the origin is

$$V_{ab}=q\frac{3ab-r^2\delta_{ab}}{r^5} . \tag{6}$$

Turning to the quantum mechanical approach, we should use an EFG operator $V_{ab}^{\mathrm{op}}=\sum V_{ab}^{\mathrm{op}}(i)$. The single-particle operator $V_{ab}^{\mathrm{op}}(i)$ is defined as

$$V_{ab}^{\mathrm{op}}(i)=-\frac{e^{3a_ib_i-r_i^2\delta_{a_ib_i}}}{r_i^5}=-\frac{e}{r_i^3}W_{ab}(i) , \tag{7}$$

where $W_{ab}(i)$ is the angular part of $V_{ab}^{\mathrm{op}}(i)$.[29] According to the density functional theory[30,31] we may write

$$\begin{aligned}V_{ab}&=-e\int V_{ab}^{\mathrm{op}}\rho(\mathbf{r})d\mathbf{r}\\&=-e\int\sum_{i=1}^{N}\psi_i^*(\mathbf{r})V_{ab}^{\mathrm{op}}(i)\psi_i(\mathbf{r})d\mathbf{r} .\end{aligned} \tag{8}$$

The wave function can be expanded into a set of basis functions

$$\psi_i(\mathbf{k},\mathbf{r})=\sum_{j=1}^{n}c_{ij}(\mathbf{k})\phi_j(\mathbf{k},\mathbf{r}) . \tag{9}$$

Using Eq. (9) and interchanging summation and integration, we obtain

$$\begin{aligned}V_{ab}&=-e\sum_{j=1}^{N}\sum_{k=1}^{N}\sum_{i=1}^{N}c_{ij}^*c_{ik}\int V_{ab}\phi_j^*(\mathbf{r})\phi_k(\mathbf{r})d\mathbf{r}\\&=-e\sum_{j=1}^{N}\sum_{k=1}^{N}n_{jk}\langle\mathbf{r}^{-3}\rangle_{jk}\int_{\Omega}Y_{l_jm_j}W_{ab}Y_{l_km_k} ,\end{aligned} \tag{10}$$

where n_{jk} is an element of the density matrix. For reasons of clarity we dropped the wave number $\mathbf{k}$.

It is our experience that the value of $\langle r^{-3}\rangle$ hardly depends on the details of the Cd environment. The EFG scales, therefore, approximately with the density matrix elements, n_{jk}, i.e., with the orbital occupation numbers [cf. Eq. (9)]. Since the occupations of the (deep) core levels do not much depend either on the Cd environment, and because for Cd in cadmium $V_{ab}(\mathrm{core})$ contributes merely 1% to the EFG,[26,32] the core contribution can be safely neglected.

In order to evaluate the lattice contribution to the EFG, we first consider a Wigner-Seitz sphere at a distance $\mathbf{R}$ from the cadmium atom. The nuclear charge is centered at $\mathbf{R}$ and the electronic charge is distributed over the sphere. The potential at the position of the cadmium atom due to the electrons in this sphere is

$$\Phi(\mathbf{R})=-e\int_{\mathrm{ws}}\frac{\rho(\mathbf{r})dr}{|\mathbf{R}-\mathbf{r}|} . \tag{11}$$

Using the Taylor expansion

$$\frac{1}{|\mathbf{R}-\mathbf{r}|}=\frac{1}{R}+\frac{\mathbf{r}\cdot\hat{\mathbf{R}}}{R^2}+\frac{3(\mathbf{r}\cdot\hat{\mathbf{R}})^2-r^2}{R^3}+\cdots \tag{12}$$

we can write the electrostatic potential in the form

$$\Phi(\mathbf{R})=\frac{q}{R}+\frac{\mathbf{P}\cdot\hat{\mathbf{R}}}{R^2}+\cdots , \tag{13}$$

where

$$q=-e\int_{\mathrm{ws}}\rho(\mathbf{r})d\mathbf{r} \tag{14}$$

is the monopole moment and

$$\mathbf{P}=-e\int_{\mathrm{ws}}\rho(\mathbf{r})\mathbf{r}\,d\mathbf{r} \tag{15}$$

is the dipole moment of the electrons inside the Wigner-Seitz sphere. The circumflex indicates a vector of unit length. The lattice contribution to the EFG follows from a simple lattice-sum calculation. We found that the dipole moments of the vacancies in the CdV_2 and CdV_3 defects contribute at most a few tenths of a percent to the EFG. Therefore, the expansion in Eq. (12) is truncated after the first term.

V. MOLECULAR STATICS AND MOLECULAR DYNAMICS SIMULATIONS

The molecular statics and molecular dynamics simulations were performed using the atom embedding method from Finnis and Sinclair.[10] The potentials needed were constructed by the method described by van der Werf *et al.*[33] We calculated the atomic positions in a tungsten lattice containing a cadmium vacancy or cadmium-vacancy-helium cluster like CdV_2, CdV_2He, CdV_2He_2, $CdV_3CdV_3He_2$, CdV_3He_3, or CdV_3He_4. Here, CdV_2

means that there are two vacancies, one of which is occupied by the cadmium atom. The initial periodic unit cell contained 2000 atoms. The atoms were allowed to move to new positions until the total energy of the cell reached a minimum value.

In Table II we give the displacements of the cadmium and helium atoms with respect to their substitutional positions, for the different defect configurations (cf. Fig. 2). It turned out that cadmium atoms in the clusters CdV_2 and CdV_2He move along the $\langle 111 \rangle$ direction towards the vacancy or the helium atom, respectively, while the helium atom in the cluster, CdV_2He moves into the opposite direction. In CdV_3, CdV_3He_2, and CdV_3He_3 clusters, the cadmium atoms are displaced in the $\langle 110 \rangle$ direction towards the two vacancies or helium atoms, respectively. The two helium atoms in CdV_3He_2 move mainly towards each other, but they stay in the $\{110\}$ plane.

The atomic positions obtained in this way are, strictly speaking, only valid at 0 K, whereas the PAC measurements were carried out while the sample was at a temperature of 300 K. Therefore, we performed dynamical simulations for the helium-decorated vacancy clusters in order to investigate the rms fluctuation of the cadmium-helium interatomic distance. The simulations covered a period of 100 ps, with time steps of 1 fs. Temperature and pressure were controlled using the method of Berendsen *et al.*[34] It turned out that the mean distance between cadmium and helium is approximately equal to the value at 0 K, and that the rms fluctuation is anisotropic and ranges from 0.10 to 0.14 Å, depending on the particular defect structure.

The configurations CdV_2He_2 and CdV_3He_4 are special. For CdV_2He_2 there are three equivalent positions of the two helium atoms (or rather six if the helium atoms are distinct). If the energy barrier is low enough, we expect the helium atoms to hop between equivalent positions with a frequency which is large compared with the quadrupole interaction frequency, in which case the PAC probe will experience a mean EFG. Therefore, we performed dynamical simulations for a number of temperatures between 300 and 600 K, covering a time interval of 50 ps in steps of 1 fs. The observed jump rate as a function of the inverse temperature is given in Fig. 1(a) in the form of an Arrhenius plot. Assuming a simple jump model, we may write

$$\nu = \nu_0 e^{-E/kT}, \tag{16}$$

where ν is the jump frequency and E is the barrier height. A least-squares fit to the data in Fig. 1(a) resulted in a barrier height $E = 0.16(2)$ eV and a frequency $\nu_0 = 9(3) \times 10^{13}$ Hz, yielding a jump frequency of about 2×10^{11} Hz at 300 K.

The situation for CdV_2He_4 is similar, but now there are two different jumps possible, each with its own energy barrier and jump frequency. We performed dynamical simulations between 300 and 1000 K covering a time interval of 100 and 200 ps in steps of 1 ps. For the two helium atoms in one of the vacancies there are two equivalent positions. The jump rate as a function of the inverse temperature is plotted in the upper part of Fig. 1(b). A least-squares fit to these data resulted in a barrier height $E = 0.19(3)$ eV and a frequency $\nu_0 = 5(3) \times 10^{13}$ Hz. This results in a jump frequency of about 3×10^{10} Hz at 300 K. In the second type of jump one of the two helium atoms in the doubly occupied vacancy moves into the other vacancy. The jump rate versus the inverse temperature is plotted in the lower part of Fig. 1. A least-

TABLE II. Displacements in Å of cadmium and helium atoms with respect to the substitutional position, for different defect configurations. The lattice constant of tungsten is 3.175 Å.

Configuration	Cd	He
CdV_2	0.17	
CdV_2He	0.12	0.06
CdV_2He	0.06	
CdV_3	0.40	
CdV_3He_2	0.18	0.11
CdV_3He_3	0.01	
CdV_3He_4	0.04	

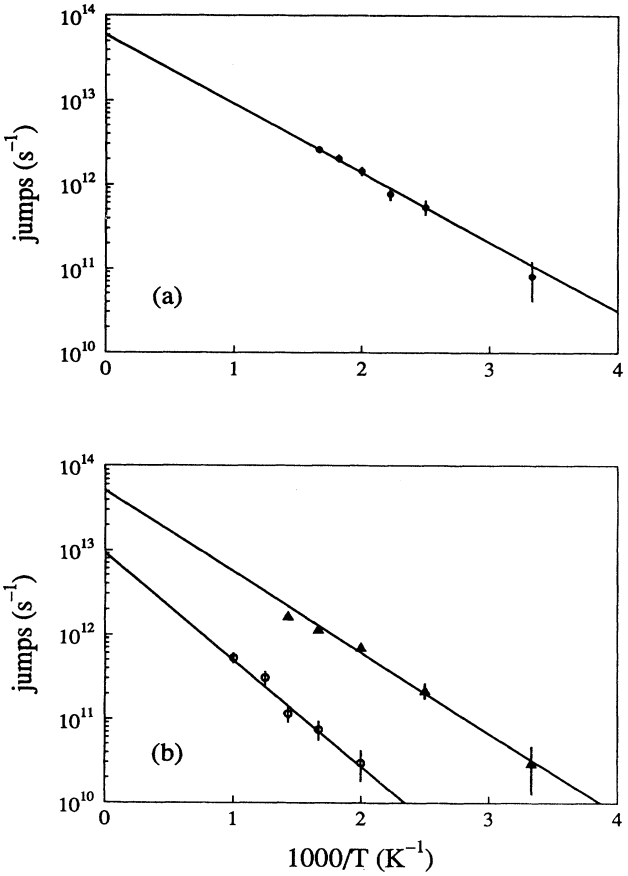

FIG. 1. Jump rate versus inverse temperature for jumps between the three equivalent helium positions in the cluster CdV_2He_2 (a), the two equivalent helium positions in the doubly occupied vacancy of the cluster CdV_3He_4 [upper curve (b)], and jumps of a helium atom from the doubly occupied to the singly occupied vacancy in CdV_3He_4 [lower curve (b)].

squares fit to this curve resulted in $E=0.25(3)$ eV and $\nu_0=9(6)\times10^{12}$ Hz, yielding a jump frequency of about 6×10^8 Hz at 300 K.

VI. EFG CALCULATIONS

In general, algorithms used for band-structure calculations fully exploit the translational and point symmetries of the crystal under consideration. When a point defect is inserted in a regular infinite crystal, there is no longer translational symmetry. This symmetry is restored in an artificial way by taking a unit cell in which the defect configuration is included. Figure 2 shows unit cells that contain a CdV_2He, CdV_3He_2, or CdV_2He_2 cluster, as used in the EFG calculations. The size of these cells is twice as large as that of the original tungsten unit cell. A point defect often reduces also the point symmetry. Cells that contain CdV_2 or CdV_2He belong to space group C_3^4, number 146 (International Tables[35]), whereas cells that contain CdV_3, CdV_3He_2, or CdV_3He_3 belong to space group C_{2v}^1, number 25. In the case of CdV_2He_2 and CdV_3He_4, the unit cell has no symmetry at all and belongs, therefore, to space group C_1^1, number 1.

In the ASW calculations, a vacancy is represented by a Wigner-Seitz sphere centered midway between the cadmium atom and the next tungsten atom in a $\langle 111\rangle$ direction. The nuclear charge within the sphere is zero, and the valence configuration in $1s2p3d$. For all atoms and vacancies we used the same sphere radius of 1.534 Å, except in the cases of CdV_2He_2, CdV_3He_3, and CdV_3He_4. The reason is that these clusters contain more atoms than substitutional lattice sites, which would cause the total volume of the spheres to be larger than the volume of the unit cell. We took the sphere radius for cadmium the same as in the other cases because the largest contribution to the EFG comes from the valence electrons (see next section). From experience one knows that the overlap of two spheres should be smaller than the overlap of two adjacent spheres in a simple cubic crystal. Therefore, we took a radius of 0.7788 Å for helium and, consequently, a radius of 1.5902 Å for tungsten in the clusters CdV_2He_2 and CdV_3He_4, and a radius of 1.6251 Å in CdV_3He_3.

We calculated the EFG for the substitutional atom positions as well as for the relaxed positions obtained in Sec. V. In the self-consistent cycle of the ASW method we scanned the irreducible part of the Brillouin zone with a **k** point density of 504–750 **k** points per Brillouin zone, depending on the symmetry of the unit cell. The (partial) density of states were evaluated with the hybrid intergration scheme of MacDonald, Vosko, and Coleridge[36] using 1475 **k** points in one-half of the Brillouin zone. When calculating the density matrix, one should choose a proper energy mesh. Figure 3 shows the total density of states for the CdV_2He_2 case. The large peak at 0.08 Ry is caused by the *d* electrons of cadmium. It is rich in structure due to the Van Hove singularities, as shown in the exploded view. In the numerical integrations this part of the density of states was sampled with an energy mesh of 0.005 mRy, while for the rest we used a mesh of 0.1 mRy.

In Table III we give the results of the EFG calculations. The contribution of the *p* electrons to V_{zz} is by far the largest, as has been observed for most hcp metals.[3,25] The lattice contribution is relatively small, typically between 1% and 5%. The *sd* contribution to the EFG of cadmium-probe atoms has, as far as we know, never been calculated before. It turned out to be of the same order of magnitude as the *d* contribution: both contribute about 10% to the total EFG, except for the configurations CdV_3He_3 and CdV_3He_4.

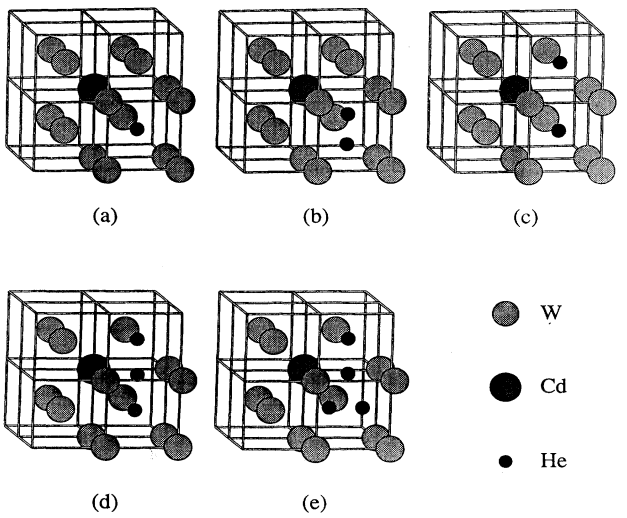

FIG. 2. The CdV_2He (a), CdV_2He_2 (b), CdV_3He_2 (c), CdV_3He_3 (d), and CdV_3He_4 (e) units cells as used in the ASW calculations.

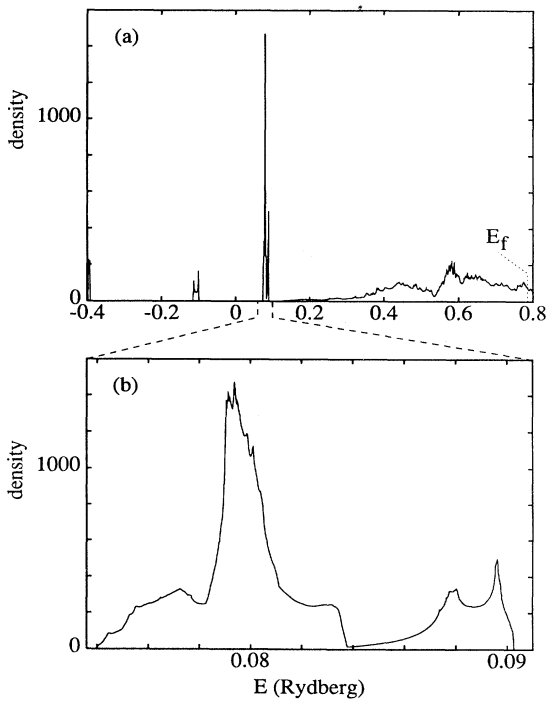

FIG. 3. Total density of states for the cluster CdV_2He_2.

TABLE III. Partial and total EFG in 10^{21} Vm^{-2}. The partial V_{zz} is the diagonalized value for the particular contribution, i.e., the PAS of the partial V_{zz} need not be the same as the PAS of the total V_{zz}. Numbers given on the first line are for the unrelaxed defect clusters; those on the second line for the relaxed configurations.

Configuration	V_{zz}^{lat}	V_{zz}^{p}	V_{zz}^{d}	V_{zz}^{sd}	V_{zz}^{tot}	η
CdV_2	0.320	7.465	−0.042	−0.499	7.24	0.00
	−0.129	14.392	−1.045	−1.068	12.15	0.00
CdV_2He	0.254	6.850	0.068	−0.566	6.61	0.00
	−0.056	10.943	−0.935	−0.879	9.07	0.00
CdV_2He_2						
	0.005	5.893	1.093	−0.241	4.87	0.44
CdV_3	−0.172	8.730	1.395	−0.566	−7.51	0.84
	0.218	13.242	−1.245	1.003	11.04	0.95
CdV_3He_2	−0.139	−7.664	1.309	−0.661	−7.09	0.52
	0.175	14.014	1.598	1.101	−12.37	0.84
CdV_3He_3						
	−0.011	7.715	−3.006	−0.335	4.38	0.85
CdV_3He_4						
	−0.013	9.295	−2.071	−0.343	7.02	0.69

In the ASW calculations for CdV_2 and CdV_2He the z axis of the coordinate system coincided with the principal z axis of the EFG. In these cases the off-diagonal elements of the EFG tensor should be equal to zero. The calculated values of these elements were of the order of 0.1×10^{21} Vm^{-2}, which indicates the size of the numerical errors.

VII. DISCUSSION

In Table IV we compare the results of our calculations with the experimental values that we previously obtained.[9] We compare quadrupole frequencies rather than EFG values because the quadrupole frequency depends on the asymmetry parameter η and because there is some uncertainty about the measured value of η in the case of CdV_3He_3.

TABLE IV. Comparison of theoretical and experimental quadrupole frequencies (Mrad s^{-1}). The column headers "relaxed" and "unrelaxed" are explained in the text.

Configuration	Unrelaxed		Relaxed		Experimental[a]	
	ω_0	η	ω_0	η	ω_0	η
CdV_2	137	0.00	230	0.00	133	0.0
CdV_2He	125	0.00	171	0.00	121	0.0
CdV_2He_2			110	0.44		
			74[b]	0.00[b]	122	0.0
CdV_3	225	0.84	356	0.95	301	1.0
CdV_3He_2	169	0.52	370	0.84		
CdV_3He_3			132	0.85	218	0.8−1
CdV_3He_4			190	0.69		
			176[b]	0.63[b]		
			184[b]	0.99[b]		

[a]Reference 9.

[b]Values averaged according to molecular dynamics simulation (see text).

The agreement between theoretical and experimental values is not quite satisfactory. Whereas the quadrupole frequencies calculated for the unrelaxed clusters CdV_2 and CdV_2He agree very well with the experimental data, the relaxed values deviate by 75% and 41%, respectively. In the case of the cluster CdV_3 both the unrelaxed and the relaxed value of the quadrupole frequency differs by about 25% from the experimental value, the unrelaxed value being too small and the relaxed value being too large.

We list two different ω_0 and η values for CdV_2He_2. The first set is valid at a temperature of 0 K, the second set should be valid at 300 K. The transition from one set to the other takes place at a temperature of about 130 K. At 300 K the two helium atoms jump at a rate which is three orders of magnitude larger than the quadrupole frequency, and the cadmium atom will experience an EFG which is due to the time-averaged superposition of the charge distributions for the three equivalent configurations.[37,38] Having calculated the EFG for one configuration, we obtain the other two by cyclic permutation of the x, y, and z indices. The asymmetry parameter obtained in this way is zero because the average charge distribution is axially symmetric. However, the quadrupole frequency at 300 K is 60% smaller than the experimental value.

It was argued that the frequency of 218 Mrads^{-1} should be assigned to the cluster CdV_3He_3.[39] The calculated quadrupole frequency for this cluster is 65% larger than the experimental one, but the asymmetry parameter is within the experimental range of values.

In Table IV we list three sets of values for the cluster CdV_3He_4. The first set is valid in the temperature range for 0 K up to the first transition temperature of about 170 K. Above this temperature the two helium atoms in the doubly occupied vacancy jump at a rate which is large compared with the quadrupole frequency, and the second set of values should be valid. At about 250 K a second transition occurs. One of the helium atoms in the doubly occupied vacancy jumps into the other vacancy at a rate which becomes larger than the quadrupole frequency, and the third set of values should be valid. The second and third set of values were obtained by averaging the proper static EFG tensors.

On the basis of the point charge model one expects an asymmetry parameter $\eta=1$ for the unrelaxed clusters CdV_3 and CdV_3He_2. This is not what we obtained from the ASW calculations (see Table IV), and only for the relaxed configuration of CdV_3 the asymmetry parameter approaches the expected value. Apparently, the value of η depends strongly on the actual atomic positions. This may explain the scatter of the experimental asymmetry parameters for CdV_3 in different bcc metals: $\eta=1.0$ in tungsten[40] and molybdenum,[41] $\eta=0.65$ in tantalum,[42] and $\eta=0.58$ in niobium.[43]

We conclude this section with a brief discussion of the most important error sources. First, even the EFG for a highly symmetric system like an hcp metal calculated with the ASW or FLAPW method[3,25] differs from the ex-

perimental value by an amount varying from 10% to 100%. This can be due to uncertainties in the quadrupole moments or to the accuracy with which the density matrix is calculated. But it may also be a consequence of the local density approximation and, in the case of ASW, the atomic sphere approximation.

Second, our calculations make it clear that relaxation of the atoms has a large impact on the quadrupole frequency as well as the asymmetry parameter. The atom embedding model and the potentials derived from it are not perfect. A slightly different potential may give rise to slightly different atom positions, which might lead to completely different values of ω_0 and η.

Third, the EFG has been calculated for $T=0$ K, but the measurements were performed at a temperature of 300 K. Because the mean atom positions at this temperature do not significantly differ from the static positions (see Sec. V), we have calculated the EFG for the mean lattice position. This value of the EFG is not necessarily the same as the value of the mean EFG for all the possible lattice positions. Experimentally, we found for CdV_2 and CdV_3 that ω_0 varies by less than 1% in the temperature range from 15 to 500 K.[39] Thus, for the undecorated defects the EFG at 0 K will be almost the same as that at 300 K. However, the calculated rms fluctuation of the cadmium-helium distance in the helium decorated defects is of the order of the static displacement (see Sec. V). Thus in this case it is not *a priori* clear that the temperature dependencies of ω_0 and η are small.

Fourth, we have used a unit cell of only twice the size of the lattice constant of tungsten. Although it is clear that the atoms close to the probe atom contribute most to the EFG [cf. Eq. (7)], we did not check if this unit cell is large enough.

VIII. CONCLUSIONS AND OUTLOOK

We have calculated electric-field gradients at the position of the cadmium atom in low-symmetry CdV_nHe_m clusters in tungsten, using the augmented spherical wave method. We were able to reproduce the experimental quadrupole frequencies within 70%, though this is not yet accurate enough to unambiguously identify the structure of the corresponding defects.

There is a large difference between the calculated EFG tensors for the relaxed and unrelaxed defect configurations. We conclude, therefore, that lattice relaxation has a large effect on both the quadrupole frequency ω_0 and the asymmetry parameter η. In this respect it is interesting to note that the value of η for the unrelaxed clusters CdV_2 and CdV_3He_2 are not equal to 1.0, as predicted by the point charge model. So, it is crucial to accurately know the atom positions in order to obtain a reliable EFG.

We predict that the cluster CdV_2He_2 has a temperature-dependent EFG with a transition temperature of about 100 K. The same holds for CdV_3He_4, but in this case there are two transitions, at about 170 K and at about 250 K, respectively. It would be worthwhile to measure the temperature dependence of ω_0 and η for these clusters.

To get insight in the error introduced by the atomic sphere approximation, the EFG calculations on the cluster CdV_2He_n should be repeated using a full potential method. The influence of the size of the unit cell should be investigated by performing calculations with a larger unit cell.

We calculated the EFG only for unrelaxed and fully relaxed systems. The effect of the position of the separate atoms in the unit cell could be studied by performing EFG calculations for a number of cadmium or helium positions in an otherwise rigid lattice. If the influence of the helium atom positions would turn out to be small, it might be possible to draw conclusions about the temperature dependence of the EFG.

The EFG of the vacancy cluster CdV_2 has been measured in nearly all the fcc and bcc metals. It would, therefore, be desirable to calculate these EFG values and compare them with the experimental results.

*Present address: Physics Department, Royal Holloway College, University of London, Egham Hill, Egham, Surrey TW20 0EX, United Kingdom.

[1]D. Wiarda, M. Uhrmacher, A. Bartos, and K. P. Lieb, J. Phys. Condens. Matter **5**, 4111 (1993).
[2]P. C. Schmidt, A. Weiss, S. Cabus, and J. Kübler, Z. Naturforsch. **42a**, 1321 (1987).
[3]R. Coehoorn, K. H. J. Buschow, M. W. Dirken, and R. C. Thiel, Phys. Rev. B **42**, 4645 (1990).
[4]B. H. Drittler, Ph.D. thesis, Forschungszentrum Jülich, 1991.
[5]B. Lindgren, Hyperfine Interact. **34**, 217 (1987).
[6]B. Lindgren, Europhys. Lett. **11**, 555 (1990).
[7]T. P. Das and P. C. Schmidt, Z. Naturforsch. **41a**, 47 (1986).
[8]A. R. Williams, J. Kübler, and C. D. Gelatt, Jr., Phys. Rev. B **12**, 6094 (1979).
[9]M. S. Abd El Keriem, D. P. van der Werf, and F. Pleiter, Phys. Rev. B **47**, 14 771 (1993).
[10]M. W. Finnis and J. E. Sinclair, Philos. Mag. A **50**, 45 (1984).
[11]E. N. Kaufmann and R. J. Vianden, Rev. Mod. Phys. **51**, 161 (1979).
[12]T. Butz, Hyperfine Interact. **52**, 189 (1989).
[13]E. Bodenstedt, U. Ortabasi, and W. H. Ellis, Phys. Rev. B **6**, 2909 (1972).
[14]F. D. Feiock and W. R. Johnson, Phys. Rev. **187**, 39 (1969).
[15]R. S. Raghavan, P. Raghavan, and J. M. Friedt, Phys. Rev. Lett. **30**, 10 (1973).
[16]R. S. Raghavan and P. Raghavan, Phys. Rev. Lett. **28**, 54 (1972).
[17]S. S. Rosenblum and W. A. Steyert, Phys. Lett. A **53**, 34 (1975).
[18]P. Raghavan, R. S. Raghavan, E. N. Kaufman, K. Krien, and R. A. Naumann, J. Phys. F **4**, L80 (1974).
[19]B. D. Geelhoed and M. N. McDermott, Phys. Lett. A **46**, 211 (1973).
[20]G. D. Sprouse, O. Häusser, H. R. Andrews, T. Faestermann, J. R. Beene, and T. K. Alexander, Hyperfine Interact. **4**, 229

(1978).
[21]N. S. Laulainen and M. N. McDermott, Phys. Rev. **177**, 1615 (1969).
[22]P. Herzog, K. Freitag, M. Reuschenbach, and H. Walitzki, Z. Phys. A **294**, 13 (1980).
[23]H. Ernst, E. Hagn, and E. Zech, Phys. Lett. A **93**, 357 (1983).
[24]J. Christiansen, P. Heubes, R. Keitel, W. Klinger, W. Loeffler, W. Sander, and W. Witthuhn, Z. Phys. B **24**, 177 (1976).
[25]P. Blaha, K. Schwarz, and P. H. Dederichs, Phys. Rev. B **37**, 2792 (1988).
[26]P. Blaha, P. Sorantin, C. Ambrosch, and K. Schwarz, Hyperfine Interact. **51**, 917 (1989).
[27]A. Lurio, Phys. Rev. **142**, 46 (1966).
[28]O. K. Andersen, Phys. Rev. B **8**, 3060 (1975).
[29]V. R. Marathe and A. Trautwein, in *Advances in Mössbauer Spectroscopy*, edited by B. V. Thosar, P. K. Iyengar, J. K. Srivastava, and S. C. Bhargava (Elsevier, Amsterdam, 1983).
[30]P. Hohenberg and W. Kohn, Phys. Rev. B **136**, 864 (1964).
[31]W. Kohn and L. J. Sham, Phys. Rev. **140**, A1133 (1965).
[32]K. Schwarz and P. Blaha, Z. Naturforsch. **47a**, 197 (1991).
[33]D. P. van der Werf, M. Breeman, H. Eleveld, A. van Veen, and R. de Groot (unpublished).
[34]H. J. C. Berendsen, J. P. M. Postma, W. F. Gunsteren, A. DiNola and J. R. Haak, J. Chem. Phys. **81**, 3684 (1984).
[35]*International Tables for Crystallography, A: Space Group Symmetry*, edited by T. Hahn (Reidel, Dordrecht, 1983).
[36]A. H. MacDonald, S. H. Vosko, and P. T. Coleridge, J. Phys. C **12**, 2991 (1979).
[37]H. Winkler and E. Gerdau, Z. Phys. **262**, 363 (1973).
[38]S. Dattagupta, Hyperfine Interact. **11**, 77 (1981).
[39]D. P. van der Werf, Ph.D. thesis, Universiteit Groningen, 1994.
[40]U. Pütz, A. Hoffmann, H. J. Rudolph, and R. Vianden, Z. Phys. B **46**, 107 (1982).
[41]A. Weidinger, R. Wessner, Th. Wichert, and E. Recknagel, Phys. Lett. A **72**, 369 (1979).
[42]H. Metzner, R. Sielemann, R. Butt, S. Klaumünzer, and W. Semmler, Hyperfine Interact. **15/16**, 413 (1983).
[43]R. Sielemann, H. Metzner, R. Butt, S. Klaumünzer, H. Haas, and G. Vogl, Phys. Rev. B **25**, 5555 (1982).